Volume 1 | Number 1 | Jan 2013 | Pages 1–100

Journal of
Materials Chemistry C

Materials for optical and electronic devices
www.rsc.org/materialsC

ROYAL SOCIETY
OF CHEMISTRY

This is an *Accepted Manuscript*, which has been through the Royal Society of Chemistry peer review process and has been accepted for publication.

Accepted Manuscripts are published online shortly after acceptance, before technical editing, formatting and proof reading. Using this free service, authors can make their results available to the community, in citable form, before we publish the edited article. We will replace this *Accepted Manuscript* with the edited and formatted *Advance Article* as soon as it is available.

You can find more information about *Accepted Manuscripts* in the [Information for Authors](#).

Please note that technical editing may introduce minor changes to the text and/or graphics, which may alter content. The journal's standard [Terms & Conditions](#) and the [Ethical guidelines](#) still apply. In no event shall the Royal Society of Chemistry be held responsible for any errors or omissions in this *Accepted Manuscript* or any consequences arising from the use of any information it contains.

Journal of Materials Chemistry C

PAPER

Polymer-Based SERS-Active Substrate with Gyroid-Structured Gold Multibranches

Han-Yu Hsueh,[a] Hung-Ying Chen,[c] Yi-Chun Ling,[d] Wei-Shiang Huang,[a] Yu-Chueh Hung,[d] Shangjr Gwo,[c] and Rong-Ming Ho*[ab]

Here, we suggest an effective method to create a three-dimensional SERS-active substrate using nanoporous polymer with bicontinuous nanochannels as a template for electroless plating of Au, giving the formation of Au multibranches with sharp tips and corners for high-density and uniformly distributed hotspots as reliable SERS devices for detection. Also, by taking advantage of easy processing for
10 polymeric materials, the polymer-based SERS-active substrate can be effectively fabricated in large area for device design with mechanical robustness. Crystal violet and β-carotene molecules are used to demonstrate the superior SERS detection sensitivity with high reproducibility and stability using the polymer-based SERS-active substrate, suggesting a new approach to fabricate materials for the detection of chemicals with average enhancement factor up to 10^8.

15 1. Introduction

Surface enhanced Raman scattering (SERS) has been explored as a powerful technique for tracing and monitoring dynamic molecular processes.[1-3] SERS is based on the field enhancement resulting from localized surface plasmon resonance
20 (LSPR) at the surface of metal substrate with plasmon resonance lying in the visible spectral range. Probe molecules can be attached to the substrates consisting of SERS-active metals to give significant SERS intensity due to the configuration of specific nanostructured metals (e.g. Ag, Au and Cu) with intense
25 LSPR, which can improve the sensitivity up to ten orders of magnitude.[4-6] Closely placed nanostructured metals would create strong local electromagnetic coupling (i.e., hotspots) at specific sites with sharper and closer geometric features, resulting in excellent SERS performance even for the detection of a single
30 molecule signal.[7-10] Nevertheless, in the applications of a practical sensor, the detection of dilute chemicals is directly related to the probability of molecules interacting with the active area of the sensor surface.[11,12] It is noted that Raman signals are usually collected from the area of approximately one to five square
35 micrometers. As a result, SERS-active substrates over the entire area with highly localized hotspots at a given time should be required to detect the chemicals for average enhancement factor (EF). While metallic colloids can be obtained by various synthetic approaches,[13-17] it is still challenging to fabricate SERS-
40 active devices with high-density hotspots and required mechanical properties since the fabricated metallic colloids are either zero-dimensional or one-dimensional. As a result, how to achieve nanostructured metals with sharper tips as ordered arrays (i.e., two-dimensional (2D) SERS-active substrates) with
45 uniformly distributed hotspots for reliable sensing has drawn

extensive attention.[18] To increase the probability of the molecules being placed near the hotspots for the enhancement of sensitivity, three-dimensional (3D) SERS-active substrates have been suggested with reliable average EF, and developed by increasing
50 the number of hotspots which are formed in the nanogaps between two neighboring metallic nanostructures (i.e., tips and corners).[19-25] Yang and co-workers fabricated a 3D SERS-active substrate by depositing Au NPs into hierarchically structured SiO_2 microcylinders. A combination of block copolymer (BCP)
55 microphase separation and microimprinting techniques enables the production of nanoporous SiO_2 structures within microscale cylinder arrays. Consequently, negatively charged Au nanoparticles (NPs) were deposited on the positively charged nanopores *via* electrostatic attraction. The resulting Au NP-
60 decorated porous microcylinders exhibit an average EF value of approximately 10^5.[22] Jeong and co-workers demonstrated a novel large-scale SERS substrate of glass nanopillar arrays with nanogap-rich Ag nanoislands, generating high density SERS hot spots within a detection volume. This SERS substrate shows high
65 average EF over 10^7 and excellent uniformity by using DNA as target molecules.[23] Chen and co-workers developed a novel wrinkled substrate with abundant "hotspots" for ultrahigh SERS enhancements by thermal contraction of pre-strained PS veneered by 100 nm nanoporous Au films. The winkling treatment turns
70 the planar nanoporous Au films to a vertical 3D nanostructure with plentiful nanogaps and sharp nanotips. The SERS enhancement of the wrinkled nanoporous Au films yield a local EF of ~10^9.[25]

In recent decades, BCPs have been comprehensively
75 investigated because of their ability to self-assemble into one-, two-, and 3D periodic nanostructures with readily adjustable size, depending on their constituted compositions and molecular weights.[26] By taking advantage of the degradable character of

BCPs, nanoporous polymers with well-ordered texture can be prepared by removal of constituted components in BCPs through ozonolysis,[27] UV degradation,[28] and reactive ion etching.[29,30] As a result, chemically degradable BCPs have played an important role for the preparation of nanoporous polymers. Also, polylactide-containing BCPs (such as polystyrene-*b*-poly(D,L-lactide) (PS-PLA)[31] and polystyrene-*b*-poly(L-lactide) (PS-PLLA)[32,33]) are highly suitable for the fabrication of nanoporous polymers because of the unstable character of ester group in polylactides, which can be hydrolytically degenerated. Most interestingly, the nanoporous polymers with well-defined nanochannels can be used as templates for templated synthesis. By exploiting the templating process, reactions such as electrochemical deposition,[34,35] electroless plating,[36,37] and sol-gel reaction[38-40] can be carried out using the BCP templates for the fabrication of nanoporous inorganic materials with precisely controlled texture after removal of the polymer template.

Here, we aim to suggest an effective method to create a 3D SERS-active substrate by using nanoporous polymer from hydrolyzed PS-PLLA with a unique geometry, double gyroid (DG), as a template for electroless plating of Au, giving the formation of nanostructured metals with sharp feature (nanosized metallic multibranches) for high-density and uniformly distributed hotspots as reliable SERS devices for detection. The DG morphology is composed of a matrix and two continuous, interpenetrating but independent networks in 3D space.[41-43] The basic shape of the gyroid is a three-fold junction of three arms, in which each arm connects to another set of three arms that are each themselves rotated to form a 3D network. Therefore, after selective degradation of the minor phase, the gyroid-forming nanostructure can be exploited to create fully interconnected nanochannels, giving the feasibility for synthesis of multibranched nanostructures when the nanochannels are filled with specific materials. Also, by taking advantage of easy processing for polymeric materials, the polymer-based SERS-active substrate can be effectively fabricated in large area for device design, and the character of soft matters with required mechanical properties is appealing for practical applications.

Figure 1 shows the schematic illustration of the fabrication of polymer-based substrate with protruded nanostructured Au from gyroid-structured air networks via templated seeding growth approach for SERS-active applications. The gyroid-forming PS-PLLA was prepared by a sequential living polymerization using a double headed initiator. Detailed synthetic routes of the PS-PLLA sample were described in our previously published results (**Figure 1a**).[32] After hydrolytic treatment, the PLLA networks can be selectively removed to give a PS matrix possessing interconnected air networks as a template (**Figure 1b**). Au particles (NPs) are grown on the inner walls of the air networks through nucleation to form Au seeds (**Figure 1c**). By controlling the reduction of Au ions (Au^{+3}), gyroid-structured Au multibranches can be fabricated (**Figure 1d**). The PS template
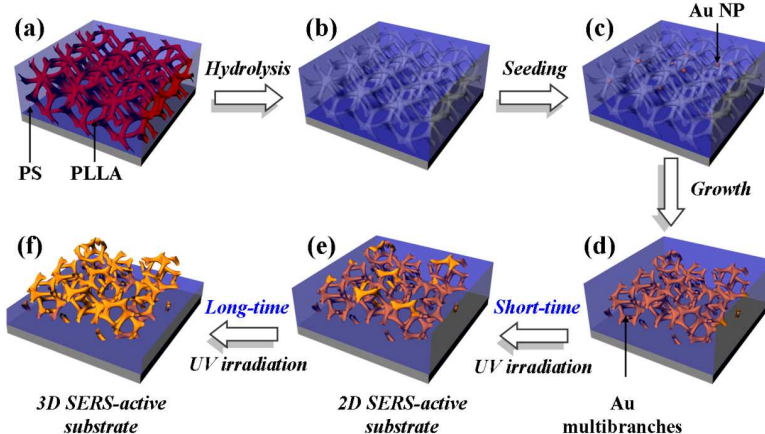

Figure 1. Schematic illustration of the fabrication of polymer-based substrate with protruded nanostructured Au from gyroid-structured air networks *via* templated seeding growth approach, followed by UV irradiation for SERS-active applications: (a) PS-PLLA thin film with two interweaved networks (PLLA (red)) in a PS matrix (blue) on a substrate (e.g. quartz); (b) Gyroid-structured nanoporous PS after removal of PLLA networks by hydrolysis; (c) Au NPs grown on the inner wall of the nanoporous PS from seeding process; (d) Multibranched Au fabricated by using the nanoporous PS decorated with the Au NPs as a template for controlled growth process; Polymer-based substrate with protruded nanostructured Au fabricated from gyroid-structured Au multibranches in the PS matrix through the degeneration of PS from the surface by (e) short-time (i.e., 24 h) and (f) long-time UV irradiation (i.e., 48 h).

can be gradually removed from the surface through UV irradiation to obtain polymer-based substrate with protruded nanostructured Au for SERS-active applications (**Figure 1e**). This templated seeding growth for synthesis of gyroid-structured Au multibranches results in homogeneous distribution of Au nanoobjects with sharp protrusion on the surface of polymer-based substrate (that is a 2D SERS-active substrate). To significantly increase the number of hotspots on the substrate, a unique approach is suggested in this study as illustrated in **Figure 1f**; the 2D SERS-active substrate is further treated by UV irradiation to give the topographic surface with higher depth (that is referred to a 3D SERS-active substrate), providing a dramatic increase in the number of hotspots in the detecting area.

2. Experimental

Synthesis of PS-PLLA BCPs

The PS-PLLA was prepared by a sequential living polymerization using a double-headed initiator. Detailed synthetic routes of the PS-PLLA sample were described in our previously published results.[32] The number-average molecular weight and the molecular weight distribution (i.e., polydispersity index) of the PS were determined by GPC. The polydispersity index (PDI) of PS-PLLA was determined by GPC and the numbers of L-LA repeating units versus styrene repeating units were determined by 1H NMR analysis. The number-average molecular weights of the PS, the PLLA and the PDI of the PS-PLLA are 34000 g mol^{-1}, 27000 g mol^{-1} and 1.21, respectively. The volume fraction of PLLA, f_{PLLA}^{v}, is thus calculated as 0.39 by assuming the densities of PS and PLLA are 1.02 and 1.248 g cm^{-3}, respectively.

Sample Preparation

Bulk samples of PS-PLLA were prepared by solution casting

from dichloromethane (CH_2Cl_2) solution (10 wt % of PS-PLLA with PLLA volume fraction, f_{PLLA}^v=0.39) at room temperature for two weeks, and then dried in a vacuum oven at 65°C for three days. The dry samples were first heated to the maximum annealing temperature, T_{max}=185°C for three minutes to eliminate the PLLA crystalline residues that were formed during the preparation procedure. After quenching from the microphase-separated, ordered melt at 180°C, the samples were prepared for SAXS experiments and then sectioned by ultra-microtome (thickness ~ 100 nm) for TEM observation. The microsections were stained by exposing to the vapor of a 4% aqueous RuO_4 solution for one hour. The RuO_4 attacks the double bonds in the PS blocks, rendering those microphase-separated domains dark in TEM due to the mass-thickness contrast. Then, the PLLA blocks of the PS-PLLA bulk samples were removed by hydrolysis, using a 0.5 M basic solution that was prepared by dissolving 2 g of sodium hydroxide in a 40/60 (by volume) solution of methanol/water. After three days of hydrolysis, the hydrolyzed samples were rinsed using a mixture of DI water and methanol, and then used as templates for following sol-gel reaction.

Templated Electroless Plating of Au

The nanoporous PS template with interconnected tortuous air network was soaked in an seeding aqueous solution mixed with methanol (20 mL) and $HAuCl_4 \cdot 3H_2O$ (0.01~0.1 g) with stirring at room temperature for several hours (3~4 hrs). After washing gently with methanol/H_2O solution to remove redundant Au ions covering on sample surfaces, the pore-filled samples were immersed into a hydrazinium hydroxide (100%, hydrazine 85 %)/methanol solution for the nucleation of Au. The diameter of Au nuclei is around 25~30 nm. By controlling the concentration of Au ions, the nucleation density of Au can be well defined. With the control of low enough Au ion concentrations, suitable amount of Au nuclei within the nanochannels of the template can be formed. Subsequently, a fresh growth solution consisting of $HAuCl_4 \cdot 3H_2O$ (0.05 g), diethanolamine (DEA, 0.1 g), HCl (1N, 0.1 mL), and methanol (20 ml) was prepared and then the pre-treated template with low content of Au nuclei was immersed into the prepared solution. Accordingly, Au ions were reduced to Au clusters arising from pre-formed Au nuclei so as to gradually develop within the nanochannels through the growth process and eventually form the PS/Au nanohybrids with preserved gyroid texture.[37] The PS/Au nanohybrids were sectioned by Leica Ultra-microtome (thickness ~ 200 nm) at room temperature for the measurement of UV-Vis absorption spectra. The microsections were collected on Quartz.

Degeneration for PS Template

To produce the nanostructured Au materials, the PS template of the PS/Au nanohybrids was degraded by exposure to UV. The degradation was carried out under atmosphere conditions using a UV source for 24 h and 48 h to obtain 2D and 3D SERS-active substrate, respectively. The intensity of the UV source was tuned for the efficient degradation of the PS matrix and did not affect the templated texture of the inorganic Au nanostructures. Exposure was to UV with a wave length of 254 nm and an intensity of 3 mW/cm^2. The PS matrix can be selectively removed through UV irradiation to obtain polymer-based substrate with protruded nanostructured Au for SERS-active applications.

SERS Measurements of nanostructured Au

The Raman measurements were performed using an optical microscope. A diode-pumped solid-state laser (Cobolt Samba) emitting at 532 nm was used as the light source. Laser was reflected from a beam splitter and focused on samples with an objective lens (Olympus, 100×, NA = 0.9). Scattered light was collected using the same objective, and then filtered for residual laser light (long pass 532, Semrock), followed with focusing on an optical fiber. This optical fiber was connected to a UV-visible spectrometer (Andor Shamrock SR-500) for data acquisition. The Raman light was dispersed using a 1200 groove/mm grating and collected on a thermoelectrically cooled CCD (DU420A, ANDOR). The same microscope and detection system was used for all spectroscopy unless otherwise noted. The experimental conditions for SERS: pumping power = 100 μW, acquisition time = 30 s.

Characterization

Bright-field transmission electron microscopy (TEM) images were obtained using the mass-thickness contrast with a JEOL JEM-2100 LaB6 transmission electron microscope (at an accelerating voltage of 200 kV). The bulk samples were sectioned at room temperature by Leica Ultra-microtome. Then, the microsections were collected on copper grids (100 mesh). The testing samples of PS-PLLA BCPs should be stained. Staining was accomplished by exposing the samples to the vapor of a 4 % aqueous RuO_4 solution for 1 hour. The RuO_4 attacks the double bonds in the PS blocks, rendering those microphase separated domains dark in TEM via mass thickness contrast. Field-emission scanning electron microscopy (FESEM) observations were performed on a JEOL JSM-6700F using accelerating voltages of 1.5-3 keV. Before observations, the samples were sputter-coated with 2-3 nm of platinum to avoid the charge effect (the platinum coating thickness was estimated from a calculated deposition rate and experimental deposition time).

3. Results and discussion

Fabrication of micrometer-thick PS-PLLA films

To fabricate polymer-based substrate with protruded nanostructured Au from suggested approach, thin-film samples with uniform and smooth surface are required. Micrometer-thick PS-PLLA films were prepared on a Quartz substrate by dip coating from PS-PLLA in 1,1,2-trichloroethane solution. The thickness of prepared polymer film can be adjusted by controlling solution concentration and dip-coating rate (**Figure S1a**). Testing samples for the following experiments were obtained by dip coating with a pulling out speed of 16 cm min^{-1} from a 20 wt% PS-PLLA in 1,1,2-trichloroethane solution, giving a thin film with thickness of 20 μm. The thickness was measured by alpha-

step profilometer, and the roughness of the testing samples was determined by tapping-mode scanning probe microscopy (SPM). The roughness of the selected surface with area of 10 μm × 10 μm is about 15 nm ($\triangle Z$ < 15 nm), providing smooth and uniform surface of thin-film samples (**Figure S1b**). **Figure S2a** shows fabricated Au NPs from low Au ion concentration (e.g. 100 ppm HAuCl$_4$ in methanol) after UV irradiation at which the Au NPs are randomly dispersed on the surface of Quartz. The diameter of Au NPs is approximately 28 nm, consistent to the TEM results, reflecting successful templating process (**Figure S2b**). To evaluate the performance of nanostructured Au for SERS, a 10 μL droplet of 10^{-8} M aqueous crystal violet (CV) solution was dropped on 1 cm^2 SERS-active substrate (see Supporting Information for details). However, the SERS results from fabricated Au NPs are not reproducible (data not shown) due to the inhomogeneous distribution of Au NPs on Quartz after UV exposure; we speculate that the inhomogeneity is attributed to low-density distribution of Au NPs. Moreover, the incomplete coverage of Au NPs will cause the formation of large-area dead zones (i.e., uncovered regions on Quartz) to reduce the probability of probed molecules in contact with metal surface for SERS performance. As a result, it is necessary to increase the nucleation density of the seeding growth of Au seeds to develop SERS-active substrate without uncovered region.

Optical Properties of Polymer-Based SERS-Active Substrate

To solve the inhomogeneity problem, higher concentration of Au ions (e.g. 106 ppm HAuCl$_4$) in methanol was used to give complete coverage of Au NPs on the PS surface. After UV
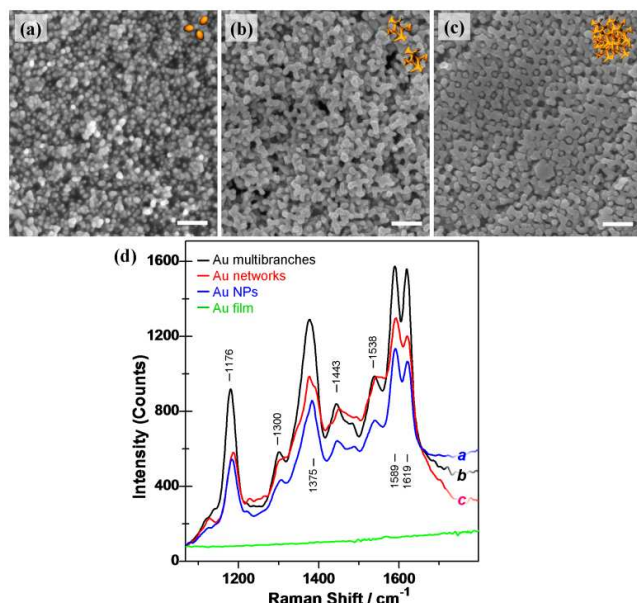

Figure 2. FESEM images of 2D SERS-active substrates composed of nanostructured Au protruding from fabricated PS/Au nanohybrids after exposure to UV irradiation: (a) Au NPs; (b) Au multibranches; (c) Au networks. The scale bar is 200 nm in length. (d) Corresponding SERS spectra of CV molecules adsorbed on the surface of the 2D SERS-active substrates composed of Au film (green line); Au NPs (blue line, curve *a*); Au multibranches (black line, curve *b*); Au networks (red line, curve *c*).

radiation, Au NPs uniformly distributed on the polymer-based substrate can be obtained as shown in **Figure 2a**. Different from

Figure S2a, dead zones can be largely reduced, giving reliable SERS performance (**Figure 2d**, curve *a*). Owing to the significant reduction in the area of dead zones, the SERS performance of the nanostructured Au on the polymer-based substrate can be greatly enhanced to give strong peaks at 1176, 1300, 1375, 1443, 1538, 1589, and 1619 cm^{-1} in the Raman spectra of the CV molecules. Note that PS molecules would not give any Raman signals, indicating that the strong Raman peaks should result from the dye molecules (**Figure S3**). Therefore, reproducible and remarkable SERS signals can be successfully acquired due to the homogeneously distributed nanostructured Au on the surface of the polymer-based substrate. By contrast, the intensity of the Raman signals for smooth Au film coated with CV molecules (**Figure 2d**, green line) is too low to be determined because of the lack of nanosized geometric texture on the smooth Au film.

To enhance the SERS performance, the Au NPs are used as seeds for the growth of Au multibranches within the DG-forming nanochannels in the PS matrix for the development of sharp tips of Au nanoobjects. With the control of reaction time for homogeneously seeding from reduction, well-defined gyroid-structured Au multibranches can be thus fabricated (**Figure S4**). Consequently, after UV irradiation for 24 h to selectively remove the PS matrix from the top of the substrate, a SERS-active substrate with homogeneously distributed gyroid-structured Au multibranches protruded from the surface of the substrate (referred as 2D SERS-active substrate) can be obtained (**Figure 2b**). The Au multibranches appear as nanoobjects with well-defined tips resembling the embryonic form of gyroid-forming nanostructure with three-fold symmetry homogeneously distributed on the PS surface, giving high areal density of tips and corners (hotspots). To quantitatively evaluate the variation of SERS efficiency from the SERS-active substrates with various nanostructured Au, the most intense Raman shift approximately at 1589 cm^{-1} (I_{1589}) ascribed to the C-C stretching vibrations of CV molecules was used for the evaluation.[44] The SERS-active substrate with Au NPs gives an I_{1589} value of 1132 counts (**Figure 2d**, curve *a*) whereas the substrate with multibranched Au gives 1575 counts (**Figure 2d**, curve *b*), indicating that the texture of the multibranched Au indeed enhances SERS performance due to the feature of the Au multibranches with high number of tips and corners. When the growth time of Au multibranches is further increased, gyroid-forming Au networks will be formed in the PS matrix. As shown in **Figure 2c**, the texture of nanoporous gyroid Au networks with three-fold symmetry can be clearly recognized after removal of the PS matrix, indicating the formation of bicontinuous Au networks. Nevertheless, the intensity of SERS from the Au networks will be reduced due to the reduction in the areal density of nanostructured tips and corners, resulting in a decrease in I_{1589} to 1297 counts (**Figure 2d**, curve *c*).

However, it is difficult to increase the density of Au multibranches even with the well control of nucleation density since high nucleation density for the growth of the Au ions will cause the formation of fragmentary texture of the Au multibranches. Therefore, a simple method to increase the number of hotspots in the detecting area from the 2D SERS-active substrate was developed. By taking advantage of the controlled degeneration of the PS matrix by UV irradiation for
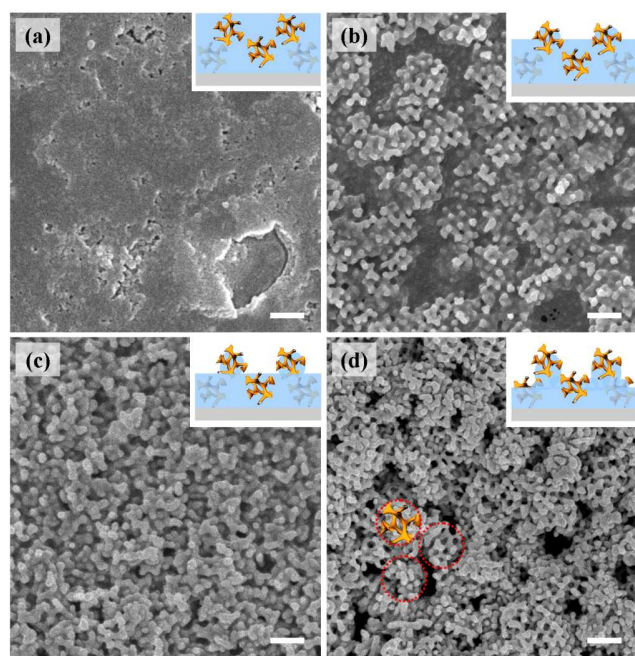
Figure 3. (a) FESEM images of gyroid-structured Au multibranches within PS matrix after UV irradiation for (a) 0h, (b) 12h, (c) 24h, and (d) 48h. Insets show the illustration of cross-section view. The red dotted circle represents the cluster of gyroid-structured Au multibranches. The scale bar is 250 nm in length.

after longer exposure time (e.g., 48 h) as shown in **Figure 3**, the feature of Au multibranches can be further surfaced out from the 2D substrate. As shown in **Figure 4**, the embryonic form of gyroid nanostructure with three-fold symmetry may extend from the top of the surface to give hierarchical texture with well-defined Au multibranches implanting into the PS matrix (i.e., 3D SERS-active substrate). Owing to the high specific surface area for the absorption of chemicals, the SERS-active substrate with increasing number of tips and corners gives superior performance in detecting. In comparison with the 2D SERS-active substrate, the SERS efficiency of the 3D SERS-active substrate can be significantly enhanced due to the larger number of hotspots, as evidenced by the outstandingly high I_{1589} value of 1934 counts (**Figure 5a**).

Average Enhancement Factor of 3D SERS-Active Substrate

To assess the performance of the SERS-active materials as sensors, Raman spectra of the CV molecules on the 3D SERS-active substrate were acquired for estimation of average EF. Note that it is impractical to use a single general definition of EF due to the diversity of situations, including single molecules, multiple molecules, experimental limitations (i.e., not knowing the exact number of molecules), average over time, spatial distribution, and the orientation of the probe on the surface.[11] As a result, different from

the EF of a single molecule (i.e., SERS enhancement from a given molecule at a specific point), the SERS EF from the whole surface area of the devices, giving the average EF, was used for the evaluation of device performance. To provide a simple method for the evaluation of the average SERS EF, the Raman measurements were performed using an optical microscope with a diode-pumped solid-state laser emitting light at 532 nm. The pumping power was 100 µW, and the acquisition time was 30 s for the SERS measurements. For reference, a 10 µL droplet of the 0.1 M aqueous CV solution was drop casted on the 1 cm × 1 cm Quartz substrate to form CV bulk for the evaluation of SERS performance.

The average EF was calculated by comparing the intensity of the chemicals from the SERS signal with that from the bulk spectra of the CV molecules using the following equation:

$$\text{EF} = \frac{I_{\text{SERS}}}{I_{\text{bulk}}} \frac{N_{\text{bulk}}}{N_{\text{SERS}}} \qquad \text{............(1)}$$

where N_{bulk} is the number of probe molecules contributing to the bulk Raman signal, N_{SERS} is the number of probe molecules contributing to the SERS signal, and I_{SERS} and I_{bulk} are the intensities of the selected scattering bands in the SERS and bulk, respectively. Since the specimens for SERS and bulk detection of CV molecules are prepared in the same way, the number of the detected molecules (N) can be estimated by following equation:

$$N = \left(\frac{N_{\text{A}} M V_{\text{solution}}}{S_{\text{sub}}} \right) S_{\text{laser}} \quad \text{.......} \quad (2)$$

where N_{A} is Avogadro constant, M is the molar concentration of the solution, V_{solution} is the volume of the droplet, S_{sub} is the size of the substrate, and S_{laser} is the size of the laser spot. Therefore, the molecule density is about 600 CV molecules per $\mu\,\text{m}^2$ (10^{-5} L of 10^{-8} M CV loaded on a 1 cm×1 cm 3D SERS-active substrate with Au multibranches) at which the laser beam size for the Raman measurements is set as large as approximately 2 µm in diameter to acquire average SERS spectra. As a result, the distribution of CV molecules on the nanostructured Au is about 1900 molecules per µm² (i.e., N_{SERS}). On the basis of the Raman scattering measurements as shown in **Figure 5a**, the I_{bulk} gives an I_{1589} value of 41 counts and the N_{bulk} is approximately $1.9×10^{10}$. Therefore, the average EF of the 3D SERS-active substrate with
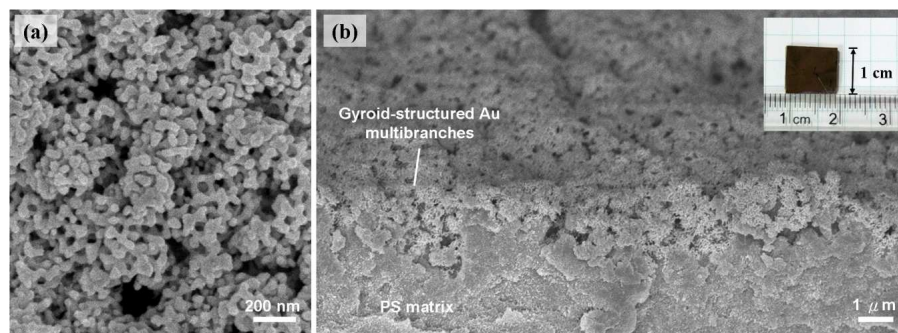

Figure 4. (a) FESEM images of top-view of 3D gyroid-structured Au multibranches. (b) Corresponding cross-section view image. Inset shows the photograph of centimeter-sized 3D SERS-active substrate.
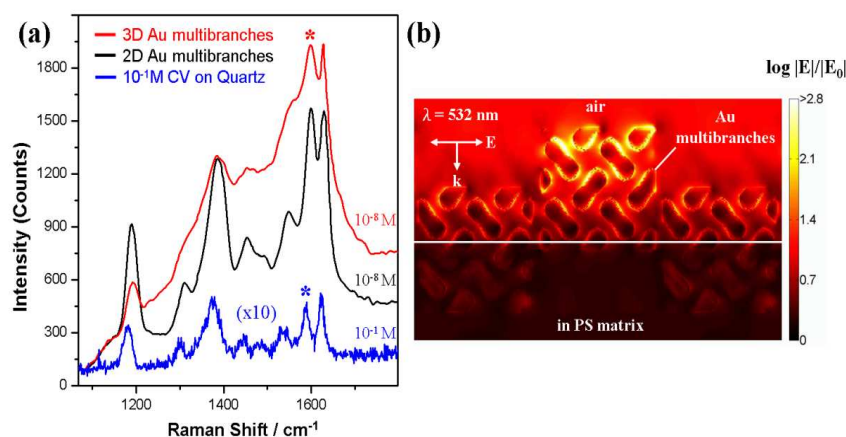
Figure 5. (a) SERS spectra of 10^{-8} M CV adsorbed on 3D (red line) and 2D (black line) SERS-active substrates with Au multibranches and CV bulk from casting of 10^{-1} M CV (blue line) on quartz substrate as reference. The Raman shift at 1589 cm^{-1} (I_{1589}) is labeled with star. (b) The electric field distribution near the hotspots of 3D SERS-active substrate is calculated from cross-section view. Note that the white line is the boundary of the PS template. The incident light at λ = 532 nm is linearly polarized. The result shows hotspots on the tips and corners of gyroid-structured Au multibranches.

Au multibranches is estimated to be approximately 4.6×10^8 at 532 nm. Raman spectra of different concentrations of CV molecules are shown in **Figure S5**. Additional optical properties including reflectance (LSPR absorption) can be provided in our previously published results.[37] The electric field was calculated on the cross section of the multibranches parallel to the polarization of incident light as shown in **Figure 5b**. The simulation was implemented using a software package Lumerical Solutions based on finite-difference time-domain (FDTD) method.[45] According to the experiment results, the dimension of gyroid-forming Au multibranches was approximated as 200 nm × 200 nm × 200 nm for each block with a lattice parameter of 100 nm. The periodic boundary conditions are used to simulate the repeated structures of multibranches, and the Lorentz-Drude model[46] was used to describe the dispersion and loss properties of gold. The geometry of the gyroid-forming multibranches can be approximated by the following function:

$$\sin x \cos y + \sin y \cos z + \cos x \sin z = t \quad ....(3)$$

where t is set to be 0.94, corresponding to a volume fraction of 39%. In order to provide a model for the rough surface of the Au multibranches, a height difference of 100 nm and a narrow gap of 20 nm between the adjacent blocks were chosen. In addition, the multibranches were embedded in a PS template (n = 1.65) with a thickness of 100 nm. The incident light was linearly polarized at 532 nm as in our experiment. The result shows a strongly enhanced local field on the tips and corners of the Au multibranches, which indicates the existence of hotspots within the structure.

Reproducibility and Stability of the SERS Substrate

To further examine the reproducibility and homogeneousness (reliability) of the performance of the 3D active-SERS substrate, The SERS spectrum of CV molecules on the substrate was randomly collected from 15 positions (**Figure 6a**). The shapes of the corresponding SERS profiles are similar to each other although their intensities show slight variation. The average SERS EF can be estimated as approximately in the order of 10^8 at 532 nm, according to the I_{1589} value (**Figure S6**), indicating the formation of uniform SERS properties across the entire area (approximately 1 cm × 1 cm). To further demonstrate the applications for sensing, the 3D SERS-active substrate was used to identify various target molecules. A droplet of ethanol solution with the 10^{-8} CV and 10^{-5} M β-carotene molecules was dropped on a testing substrate for SERS characterization. The SERS performance of β-carotene molecules absorbed on the 3D SERS-active substrate can be enhanced to give scattering peaks at 963, 1008, 1158, 1191, 1278, 1445, and 1524 cm^{-1} (**Figure S7**).[47] Note that the use of higher concentration of β-carotene molecule in the testing solution with target molecule than that of CV molecule for SERS signals is attributed to the weaker bonding of β-carotene molecule on the Au metal surface so that only pre-exposed molecules are able to be responsible for SERS signals. **Figure 6b** shows the characterization of SERS spectra of mixed CV and β-carotene molecules absorbed on the 3D SERS-active substrate. The SERS peaks resulting from the CV molecule marked with diamonds at 1176, 1538, 1589, and 1619 cm^{-1} can be clearly observed while the SERS peaks at 1158 and 1524 cm^{-1} attributed to the β-carotene molecule are marked with circles, demonstrating that the 3D SERS-active substrate can be applied for detection of various target molecules. Furthermore, recyclable application was examined by cleaning the target molecules absorbed on the substrate and addressing a renewable SERS-active substrate for detection. **Figure 6c** shows the results of recyclable application of the 3D SERS-active substrate for the CV and β-carotene molecules. Ethanol solution containing CV molecule was first drop casted on the 3D SERS-active substrate for SERS spectra. Subsequently, the testing substrate was soaked in Fe^{+2}/H_2O_2 solution (i.e., Fenton reaction) followed by exposure to UV irradiation to remove residual molecules for renewing SERS-active substrate. Consequently, β-carotene molecule was used for following SERS characterization. The main bands of CV molecule will be diminished, and the new SERS peaks from β-carotene molecule will appear. The intensities of Raman scattering for the corresponding target molecules remain the same independent of the recycled number, indicating that the 3D SERS-active substrate can be repeatedly used as detector to trace the target molecule.
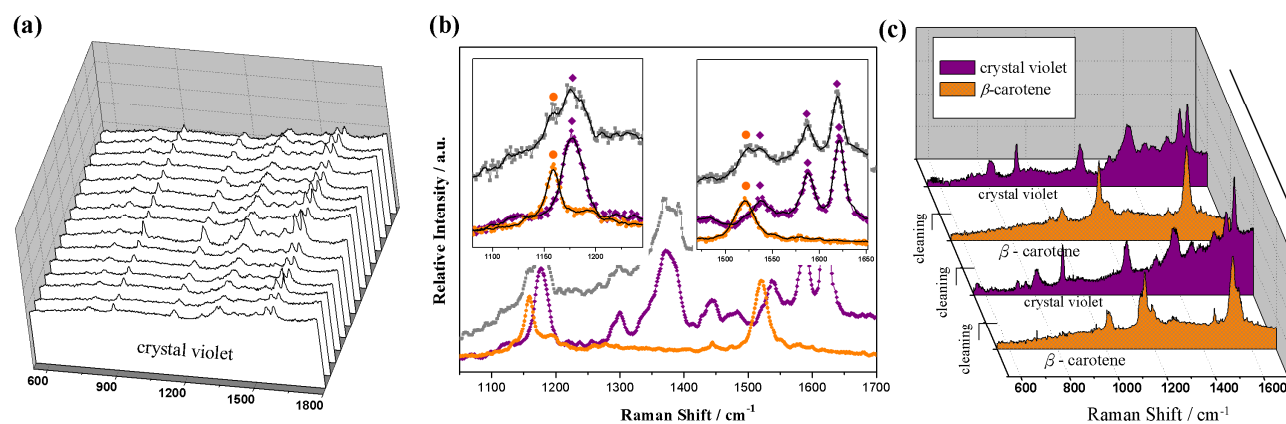
4. Conclusions

Figure 6. (a) SERS spectra of 10^{-8} M CV molecules collected on fifteen randomly selected places of a 3D SERS-active substrate. (b) Characterization of SERS spectra of CV (10^{-8} M) and β-carotene (10^{-5} M) molecules co-deposited on 3D SERS-active substrate (-■- solid square). The solid diamonds (◆) and circles (●) show the main SERS peaks of CV (-□-) and β-carotene (-●-) molecules, respectively. Insets show the enlarged area of Raman shift from 1080 to 1245 cm^{-1} and 1470 to 1650 cm^{-1}. (c) Reversible SERS behavior of 3D SERS-active substrate composed of Au multibranches with two cycles for CV and β-carotene molecules, respectively.

In conclusion, nanoporous polymer with DG-forming nanochannels can be fabricated from the self-assembly of degradable BCP (PS-PLLA) followed by hydrolysis of PLLA blocks. The nanoporous polymer can be served as a template for
5 following templated electroless plating to fabricate gyroid-structured Au multibranches, resulting in homogeneous distribution of Au nanoobjects with sharp protrusion on the surface of polymer-based substrate (that is a 2D SERS-active substrate) after UV irradiation. Significant improvement on the
10 SERS performance can be achieved due to the specific feature of the Au multibranches with high number of tips and corners. A 3D SERS-active substrate can be fabricated from the 2D one by further UV irradiation treatment, giving the high areal density of hotspots due to the high specific surface area for the absorption of
15 chemicals for the enhancement of sensitivity. CV and β-carotene molecules were used to demonstrate the superior SERS detection sensitivity with high reproducibility and stability using the SERS-active substrate with gyroid-structured Au multibranches. These polymer/metal nanohybrids allow the fabrication of polymer-
20 based SERS-active devices with mechanical robustness and chemical stability to provide protection from the surrounding environments. The high performance of this polymer-based SERS-active substrate with gyroid-structured Au multibranches suggests a new approach to fabricate materials for molecule
25 detection with average enhancement factors up to 10^8.

Acknowledgements

35 Notes and references

^{a} Department of Chemical Engineering, National Tsing-Hua University, Hsinchu, Taiwan, 30013, R.O.C E-mail: rmho@mx.nthu.edu.tw.
^{b} Frontier Research Center on Fundamental and Applied Sciences of Matters, National Tsing Hua University, Hsinchu 30013, Taiwan
40 ^{c} Department of Physics, National Tsing Hua University, Hsinchu, Taiwan, 30013, R.O.C
^{d} Institute of Photonics Technologies, National Tsing Hua University, Hsinchu, Taiwan, , 30013, R.O.C
†Electronic Supplementary Information (ESI) available: Text giving
45 detailed experimental section See DOI: 10.1039/b000000x/

1. M. Fleischman, P. J. Hendra, A. J. McQuillan, *Chem. Phys. Lett.* 1974, **26**, 163.
2. D. L. Jeanmaire, R. P. Van Duyne, *J. Electroanal. Chem.* 1977, **84**,
50 1.
3. M. G. Albrecht, J. A. Creighton, *J. Am. Chem. Soc.* 1977, **99**, 5215.
4. Y. Fang, N. H. Seong, D. D. Dlott, *Science* 2008, **321**, 388.
5. T. K. Sau, A. L. Rogach, F. Jäckel, T. A. Klar, J. Feldmann, *Adv. Mater.* 2010, **22**, 1805.
55 6. V. Lierman, C. Yilmaz, T. M. Bloomstein, S. Somu, Y. Echegoyen, A. Busnaina, S. G. Cann, K. E. Krohn, M. F. Marchant, M. Rothschild, *Adv. Mater.* 2010, **22**, 4298.
7. A. Polman, *Science* 2008, **322**, 868.
8. M. J. Banholzer, J. E. Millstone, L. Qin, C. A. Mirkin, *Chem. Soc.*
60 *Rev.* 2008, **37**, 885.
9. P. J. Schuck, D. P. Fromm, A. Sundaramurthy, G. S. Kino, W. E. Moerner, *Phys. Rev. Lett.* 2005, **94**, 017402-1.
10. D. K. Lim, K. S. Jeon, M. H. Kim, J. M. Nam, Y. D. Suh, *Nat. Mater.* 2010, **9**, 60.
65 11. E. C. Le Ru, E. Blackie, M. Meyer, P. G. Etchegoin, *J. Phys. Chem. C* 2007, **111**, 13794.
12. D. He, B. Hu, Q. F. Yao, K. Wang, S. H. Yu, *ACS Nano* 2009, **3**, 3993.
13. J. P. Xie, Q. B. Zhang, J. Y. Lee, D. I. C. Wang, *ACS Nano* 2008, **2**,
70 2473.
14. Y. N. Xia, Y. J. Xiong, B. Lim, S. E. Skrabalak, *Angew. Chem. Int. Ed.* 2009, **48**, 60.
15. N. Pazos-Perez, C. S. Wagner, J. M. Romo-Herrera, L. M. Liz-Marzán, F. J. García de Abajo, A. Wittemann, A. Fery,* R. A.
75 Alvarez-Puebla, *Angew. Chem. Int. Ed.* 2012, **51**, 12688.
16. R. A. Alvarez-Puebla, L. M. Liz-Marzán, *Angew. Chem. Int. Ed.* 2012, **51**, 11214.
17. L. F. Zhang, S. L. Zhong, A. W. Xu, *Angew. Chem. Int. Ed.* 2013, **52**, 645.
80 18. Y. Wang, M. Becker, L. Wang, J. Q. Liu, R. Scholz, J. Peng, U. Gosele, S. Christiansen, D. H. Kim, M. Steinhart, *Nano Lett.* 2009, **9**, 2384.
19. C. C. Fu, A. Grimes, M. Long, C. G. L. Ferri, B. D. Rich, S. Ghosh, L. P. Lee, *Adv. Mater.* 2009, **21**, 4472.

20.   L. Y. Chen, J. S. Yu, T. Fujita, M. W. Chen, *Adv. Funct. Mater.* 2009, **19**, 1221.
21.   S. Yang, K. Khare, P. C. Kin, *Adv. Funct. Mater.* 2010, **20**, 2550.
22.   S. Y. Lee, S. H. Kim, M. P. Kim, H. C. Jeon, H. Kang, H. J. Kim, B. J. Kim, S. M. Yang, *Chem. Mater.* 2013, **25**, 2421.
23.   Y. J. Oh, K. H. J, *Adv. Mater.* 2012, **24**, 2234.
24.   M. Alba, N. Pazos-Perez, B. Vaz, P. Formentin, M. Tebbe, M. A. Correa-Duarte, P. Granero, J. Ferré-Borrull, R. Alvarez, J. Pallares, A. Fery, A. R. de Lera, L. F. Marsal, R. A. Alvarez-Puebla, *Angew. Chem. Int. Ed.* 2013, **52**, 6459.
25.   L. Zhang, X. Y. Lang, A. Hirata, M. W. Chen, M. Chen, *ACS Nano*, 2011, **5**, 4407.
26.   F. S. Bates, G. H. Fredrickson, *Annu. Rev. Phys. Chem.* 1990, **41**, 525.
27.   M. Park, C. Harrison, P. M. Chaikin, R. A. Register, D. H. Adamson, *Science* 1997, **276**, 1401.
28.   T. Thurn-Albrecht, R. Steiner, J. DeRouchey, C. M. Stafford, E. Huang, M. Bal, M. Tuominen, C. J. Hawker, T. P. Russell, *Adv. Mater.* 2000, **12**, 787.
29.   J. Y. Cheng, C. A. Ross, V. Z. H. Chan, E. L. Thomas, R. G. H. Lammertink, G. J. Vancso, *Adv. Mater.* 2001, **13**, 1174.
30.   C. C. Chao, T. C. Wang, R. M. Ho, P. Georgopanos, A. Avgeropoulos, E. L. Thomas, *ACS Nano*, 2010, **4**, 2088.
31.   A. S. Zalusky, R. Olayo-Valles, C. J. Taylor, M. A. Hillmyer, *J. Am. Chem. Soc.* 2001, **123**, 1519.
32.   R.-M. Ho, Y.-W. Chiang, C.-K. Chen, H.-W. Wang, H. Hasegawa, S. Akasaka, E. L. Thomas, C. Burger, B. S. Hsiao, *J. Am. Chem. Soc.* 2009, **131**, 18533.
33.   R. M. Ho, W. H. Tseng, H. W. Fan, Y.-W. Chiang, C. C. Lin, B. T. Ko, B. H. Huang, *Polymer* 2005, **46**, 9362.
34.   E. J. W. Crossland, M. Kamperman, M. Nedelcu, C. Ducati, U. Wiesner, D. M. Smilgies, G. E. S. Toombes, M. A. Hillmyer, S. Ludwigs, U. Steiner, H. J. Snaith, *Nano Lett.* 2009, **9**, 2807.
35.   M. R. J. Scherer, L. Li, P. M. S. Cunha, O. A. Scherman, U. Steiner, *Adv. Mater.* 2012, **24**, 1217.
36.   H. Y. Hsueh, Y. C. Huang, R. M. Ho, C. H. Lai, T. Makida, H. Hasegawa, *Adv. Mater.* 2011, **23**, 3041.
37.   H. Y. Hsueh, H. Y. Chen, Y. C. Hung, Y. C. Ling, S. Gwo, R. M. Ho, *Adv. Mater.* 2013, **25**, 1780.
38.   W. H. Tseng, C. K. Chen, Y. W. Chiang, R. M. Ho, S. Akasaka, H. Hasegawa, *J. Am. Chem. Soc.* 2009, **131**, 1356.
39.   H. Y. Hsueh, H. Y. Chen, M. S. She, C. K. Chen, R. M. Ho, S. Gwo, H. Hasegawa, E. L. Thomas, *Nano. Lett.* 2010, **10**, 4994.
40.   H. Y. Hsueh, R. M. Ho, *Langmuir* 2012, **28**, 8518.
41.   D. A. Hajduk, P. E. Harper, S. M. Gruner, C. C. Honeker, G. Kim, E. L. Thomas, L. J. Fetters, *Macromolecules* 1994, **27**, 4063.
42.   M. F. Schulz, F. S. Bates, K. Almdal, K. Mortensen, *Phys. Rev. Lett.* 1994, **73**, 86.
43.   M. W. Matsen, M. Schick, *Phys. Rev. Lett.* 1994, **72**, 2660.
44.   M. V. Cañamares, C. Chenal, R. L. Birke, J. R. Lombardi, *J. Phys. Chem. C*, 2008, **112**, 20295.
45.   Lumerical Solutions, Inc. http://www.lumerical.com.
46.   D. Rakic, A. B. Djurisic, J. M. Elazar, M. L. Majewski, *Appl. Opt.* 1998, **37**, 5271.
47.   J. S. Vrettos, D. H. Stewart, J. C. de Paula, G. W. Brudvig, *J. Phys. Chem. B*, 1999, **103**, 6403.
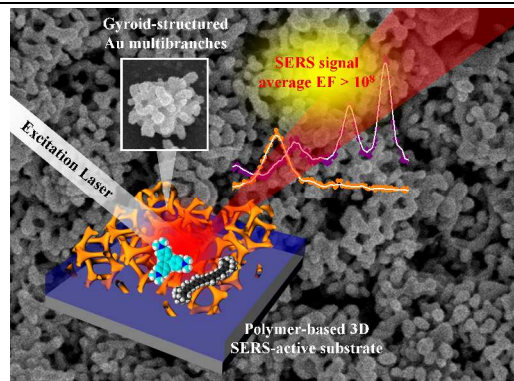
SYNOPSIS TOC: Here, we suggest an effective method to create a three-dimensional SERS-active substrate by using nanoporous polymer from hydrolyzed PS-PLLA with a unique geometry, double gyroid, as a template for electroless plating of Au, giving the formation of gyroid-structured Au multibranches with sharp tips and corners for intense hotspots and uniformly distributed hotspots for reliable measurements as SERS detectors. Also, by taking advantage of easy processing for polymeric materials, the polymer-based SERS-active substrate can be effectively fabricated in large area for device design, and the character of soft matters with required mechanical properties is appealing for practical applications. Crystal violet and β-carotene molecules are used to demonstrate the superior SERS detection sensitivity with high reproducibility and stability using the polymer-based SERS-active substrate, suggesting a new approach to fabricate materials for molecule detection with ultrahigh SERS enhancement factor (EF as high as 10^8).